Instrument Science Report WFC3 2018-14

Focus-Diverse PSFs for Five Commonly Used WFC3/UVIS Filters

Jay Anderson

October 4, 2018

Abstract

Using the techniques introduced in Anderson & Bedin (2017), we have constructed focus-diverse PSF models from `_flc` images for UVIS' most commonly used filters: F275W, F336W, F438W, F606W, and F814W. To do this, we went through the entire WFC3/UVIS archive and identifed exposures that had a moderate density of stars across the detector. We compared the star images in each exposure to a "library" PSF to come up with a "Delta PSF" model for each exposure. We intercompared these Delta PSFs and used a self-organizing strategy to group similar PSFs together. We found that this led to a natural ordering of the PSFs along a single curve, which can be parametrized by an empirical focus value. We then constructed a fully spatially variable PSF for a variety of fiducial focus levels. We will soon make these PSFs available to the public, along with a tool that can identify the focus level for any exposure (along with the best-fit PSF), provided the image contains at least five moderately bright star images.

1. Introduction

The point-spread function (PSF) is the transfer function that stands between us and perfect detection of the universe. The scene that is delivered to the telescope is convolved by the instrument optics then collected in the detector pixels to produce the images that we observe. HST's PSFs are considerably more stable than PSFs from the ground, so if we can solve for this modulating kernel, we can do much more effective comparisons between theory and data.

Despite the value of understanding HST's PSF, a good model has thus far been elusive. There are several reasons for this. Firstly, it is not easy to construct an accurate model. The detector is undersampled in many of the filters, which means that a single exposure can give us only an incomplete picture of the scene and of the PSF itself. Secondly, the PSF changes with position on the detector, on account of both material variations across the detector and changes in the geometrical optics with location in the focal plane. Finally, the PSF also changes with focus. Most exposures are taken near the focus sweet-spot, but many are too far out of focus to assume a nominal PSF. A quantitative study of how much time the PSF spends at off-nominal focus locations has never been done. The current procedure for determining PSF focus (phase retrieval) requires dedicated external observations, and as such cannot be done as regularly as one might desire PSF information.

For all the above reasons, it has taken longer than one might hope to develop a comprehensive useful model of the HST PSF. But one other reason is less obvious: even if we had a perfect model of the HST PSF, it would be hard to use. In many cases, to do high-precision PSF analyses, we need to be able to analyze the pixels simultaneously in a dithered set of images if we hope to put all the constraints on the scene together. This not only requires having a high-precision PSF, but it also requires a high-precision distortion solution and similarly precise image-to-image transformations. So, an accurate PSF will only be maximally useful to the community when other tools are also available as well.

Over the last few years, the WFC3 group has been working simultaneously on all these interrelated issues with an aim to both provide PSFs and software to use them. An additional benefit of having a set of focus-diverse PSFs is that it will be easier to monitor the PSF. We can finally use all external exposures that have a few moderately bright stars (which includes almost all half-orbit exposures) to determine a reliable estimate of the telescope's effective average focus during the exposure. In addition to helping users, this will also help Goddard engineers determine when it is best to make focus adjustments.

2. Showing the way: Anderson & Bedin (2017)

As mentioned above, understanding the HST PSF has been a longstanding challenge. In a 2015 ISR, Anderson et al. (A15) made use of the fact that the upper left corner of the WFC3/UVIS detector is more sensitive to focus than the rest of the detector and studied a set of images that contained a large number of stars in that region. We overcame the undersampling challenge by restricting our study to stars that were centered on pixels. This allowed us to make a direct empirical measurement of the PSF asymmetry. We were able to verify that on one side of focus, the PSF has an elongation in the 45° direction, but on the other side of focus, that elongation is along the 135° axis. While this behavior was expected, the fact that it could be seen directly in the images without recourse to complicated phase-retrieval software gave us encouragement that it might be possible to construct an empirical model of how the PSF changes with focus.

The next step was to explore the variation of the PSF across the detector. Although the variation with focus is greatest in the upper-left corner, in practice the PSF does vary considerably with focus everywhere on the detector. To study this, we need a set of images that have a "goldilocks" density of stars across the detector. By this, we mean there must be enough good

S/N stars to explore the PSF in each 500×500-pixel zone, but not so many stars that there is significant crowding (which can make it hard to extract a PSF out to a radius of 10 pixels).

It so happened that a there exists such a data set for globular cluster M4: GO-12911 (PI-Bedin). The program obtained about 50 exposures through the F467M filter of the broad core of the cluster once a month for a total of 589 exposures. There were about 5000 well-exposed stars in each exposure. The goals of the program involved using high-precision astrometry to look for signs of "wobble" in the motions of the stars, which might indicate unseen massive companions. Thus, having an exquisitely accurate PSF model was critical.

In Anderson and Bedin (2017, AB17), we constructed a focus-diverse set of PSFs for this data set. We started by creating an average "library" PSF that was representative of the average state of the telescope. The WFC3/UVIS PSF changes with position on the detector with a coherence scale of about 500 pixels, so we treated the spatial variability with an array of 7×4 PSFs across each 4096×2048 chip, **Figure 1** below shows the fiducial locations of the PSFs. To get a PSF anywhere on the detector, we simply used linear interpolation between the neighboring PSFs. We placed PSFs at the edges and corners so that we would never have to extrapolate. Each individual PSF is 4×-supersampled representation of how the light of a point-source is distributed among its inner 12.5 pixels. See Anderson 2016 for more details.

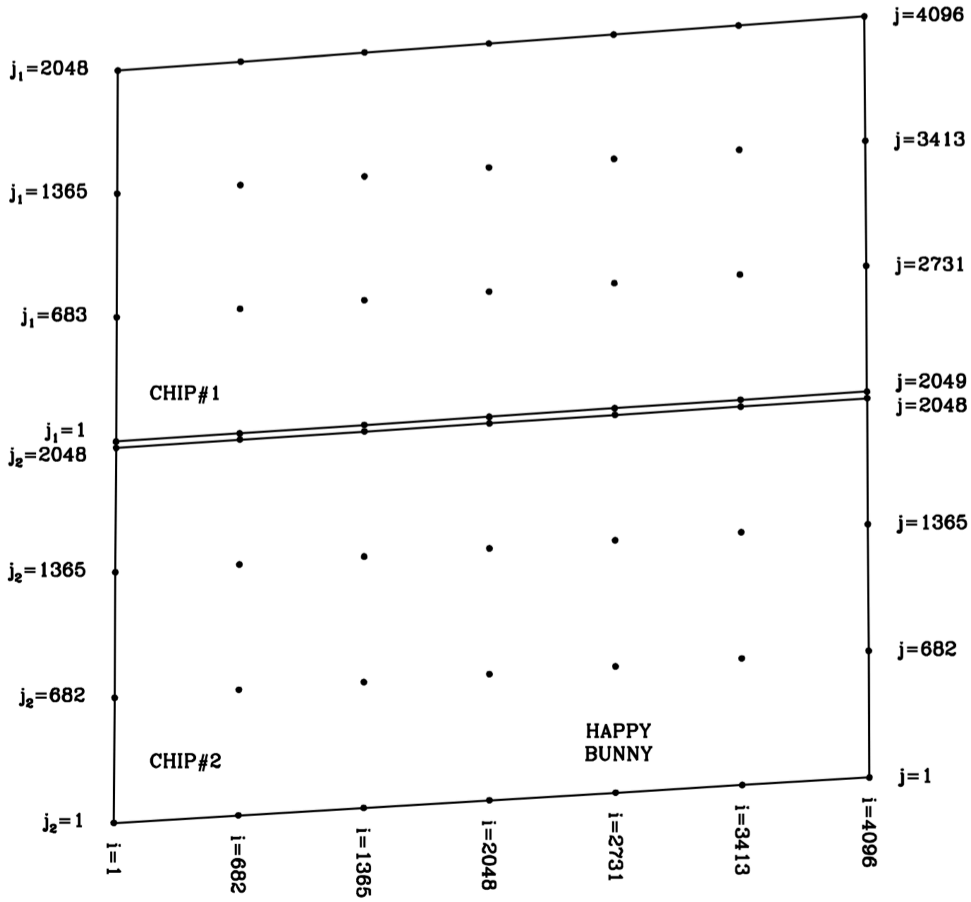

Figure 1: The locations for the 7×8 fiducial PSFs spread across the two chips of the UVIS detector. Pixel locations are given for each chip on the left, and for a vertically abutted system on the right. The "happy bunny" region described in Sabbi & Bellini (2015) is noted.

The next step was to fit the time-averaged but spatially-variable PSF to the stars in each exposure. We then studied the residuals to these PSF-fitted stars and distilled them into a 4×4 array of residual PSFs across the detector, with the outermost gridpoints placed at the edges of the detector, analogous to **Figure 1**. Much of the PSF's spatial variability comes from variations in chip-thickness and geometric optics, so treating the focus-related variations with less positional resolution is not a problem. We interpolated this 4×4 array of residual PSFs to the 7×8 fiducial library-PSF grid (shown in Figure 1) and added them to the library PSF to get the full spatially variable PSF for each exposure. In this way, we arrived at a tailor-made PSF for each of the 589 exposures.

We then inter-compared the PSFs for the various exposures and constructed a simple metric to calibrate the difference between them. We took the absolute value of the difference between the PSFs of every pair of images (589×588/2 = 173,166 unique pairs), and this gave us some handle on which PSFs are more similar to each other, and which are more different. We used this metric to arrange the exposures on a two-dimensional grid in a manner akin to that of "phylograms" from biology, which represent the same concept but for DNA to show how closely various species are related to each other. The PSFs are found to "self-organize" into a one-parameter family, which happened to look quite a lot like the banana plots of A15.

We then identified eleven distinct zones of focus along this curve and grouped the exposures by focus zone. We then took all the exposures in each zone and constructed a complete PSF for each one — this means a full set of 7×8 PSFs arrayed across the detector as in **Figure 1**. We then gathered all of these PSFs into a single fits file, a meta-PSF framework that allows us to fit the stars in an image with PSFs from the different focus levels to determine which focus level best corresponds to the stars in the exposure.

It turned out that we needed only 5 decently bright (S/N>30) stars in an exposure to definitively determine the focus level that is most appropriate for that exposure. This allowed us to identify the PSF for each exposure and also allowed us to explore how the focus varied with time, from exposure to exposure. We saw that the focus sometimes changes regularly from exposure to exposure and from orbit to orbit, but sometimes it changes irregularly.

This focus measurement is purely empirical. Nevertheless, if we combine it with phase-retrieval data, it could in principle be calibrated into offsets from the optimal positioning of the HST secondary mirror, which can be moved to compensate for the long-term shrinkage of the HST optical bench. See Niemi et al. (2010).

3. Identification of Usable Images

The goal of this ISR is to extend the effort of Anderson & Bedin (2017) for the F467M filter of GO-12911 to the full WFC3 archive for the five most commonly used filters: F275W, F336W, F438W, F606W, and F814W.

Not all images can contribute to our understanding of the PSF. This section will detail how I searched the archive to determine which images can contribute to our understanding of the PSF. Specifically, the images must have at least ~25 stars in each 4×4 region of the image, so that an array of "Delta PSFs" can be constructed to reflect the differences between the image's PSF and that of the static library PSF.

The WFC3/UVIS team archives every exposure that has been taken by HST over its lifetime on a filesystem at the Institute. We ran a simple star-finding routine on each exposure taken through F275W, F336W, F438W, F606W, and F814W using static "library" PSFs extracted from exposures taken of the center of Omega Centauri taken during commissioning. We then identified the exposures that had an even distribution of stars across the exposure to allow us to study the spatially variable PSF. Table 1 shows the results of this search.

Filter	**Total Exposures**	**Usable Exposures**
F275W	2916	471
F336W	1138	482
F438W	1074	474
F606W	4783	1470
F814W	4907	1716

There are thus many hundreds of exposures in each filter that have enough stars to allow us to characterize the PSF in that exposure. In the next section, we will extract and examine these PSFs.

4. The Focus Curve for F275W

We made a list of the 471+ qualifying exposures for each filter and re-requested them from the archive (the WFC3 team's local archive is not kept current with the latest reference files). We then ran the same star-finding routine on them and extracted a 3×3 "delta" PSF for each exposure[1].

Figure 2 below shows the ΔPSFs for the first eight out of 471 F275W exposures. It is clear that the PSF changes from exposure to exposure, but it does not do so in completely random ways: the second and eight PSF's look quite similar, for example.

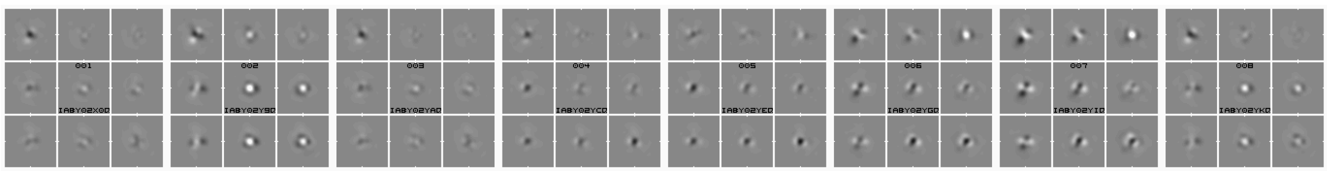

Figure 2: The 3×3 "delta" PSFs for the first eight F275W exposures. The 3×3 array represents the ΔPSF at the center, 4 edges and 4 corners of each exposure. Dark represents locations in the star image where there is more flux than predicted by the "library" model.

We have 471 such delta PSF images for the F275W filter. As we did in AB17, we construct a metric to tell us how similar the PSFs are to one another. Here, for simplicity, instead of combining the delta PSFs with the library PSFs to get a total PSF, we simply constructed the difference between the delta PSFs for images N and N′: $d_{NN'} = \sum_{LM}\sum_{ij}\left|\Delta PSF_{ij;LM;N} - \Delta PSF_{ij;LM;N'}\right|/9/16$, where the sum over (i,j) is over the inner 5×5 image pixels of each individual delta PSF, L and M correspond to the 3×3 array of spatial PSFs. N and N′ correspond to two different exposures. The division by 9 and 16 take into account, respectively, the 3×3 PSF array and the 4× super-sampling of the effective PSF (in two dimensions).

With the 471 exposures, we thus construct 471×470/2 unique pair-wise difference metrics. The units of this metric correspond to the amount of flux that would have to be transferred from one PSF to match the other. Thus, a $d_{NN'}$ of 0.1 would correspond to a pair of PSFs that differed by 10% in terms of where the flux was distributed.

AB17 shows how we can organize these into "phylogram"-type plots, wherein the exposures are placed into a two-dimensional space such that their distance from one another most closely corresponds to the $d_{NN'}$ between them. AB17 describes in detail the procedure that is used to arrive at these plots.

[1] We determined that a 3×3 array of residual PSFs gave us more stars to work with for each one and was better for our purposes than the 4×4 array used in AB17.

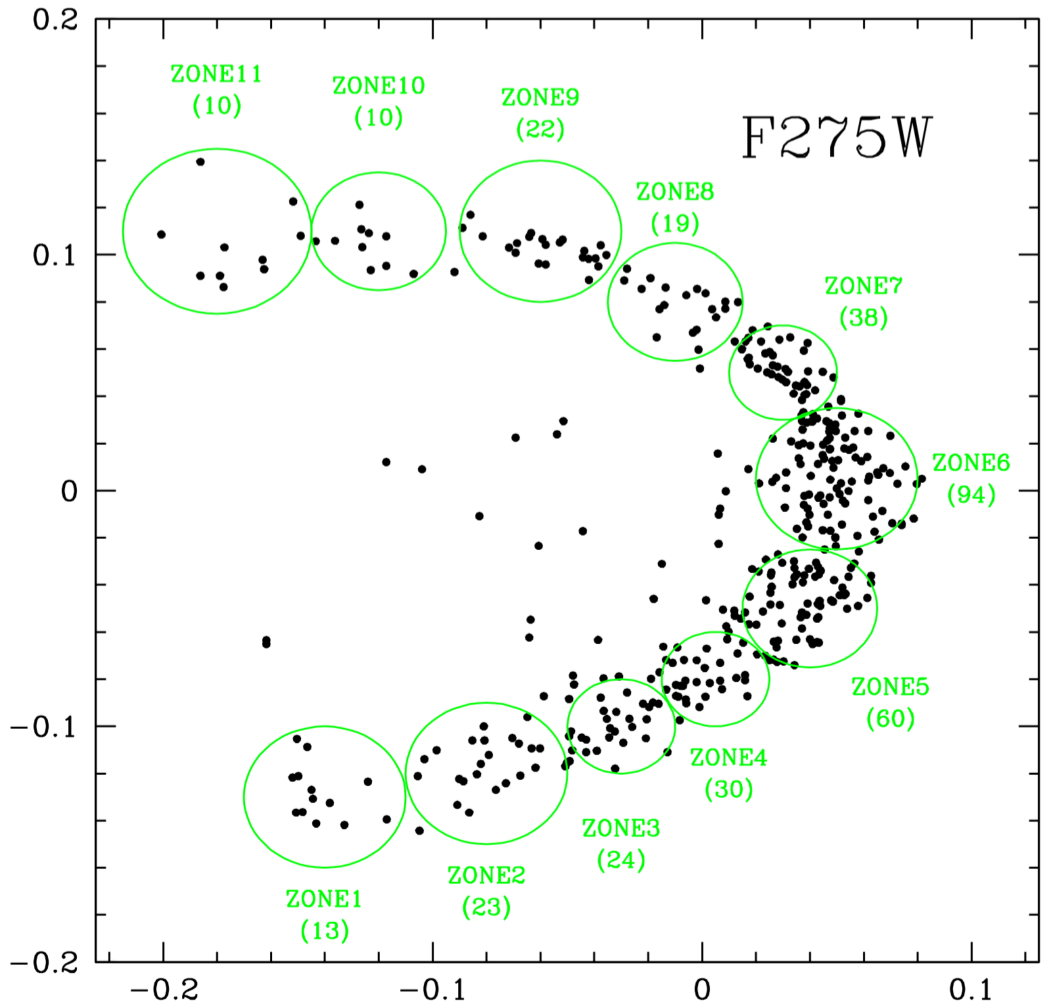

Figure 3: The "phylogram" type plot for the F275W PSF. Each of the 471 F275W exposures is shown as a dot in this figure. The focus zones are identified by green circles.

Figure 3 shows the phylogram plot for F275W. Each dot in the figure corresponds to one of the 471 exposures. The axes are arbitrary, but the distance from one point to the other is optimized to represent as well as possible the difference between the two PSFs.

Just as AB17 saw for the F467M PSF, the F275W PSFs "self-organize" into a single-parameter family, where the parameter is likely to be related to the focus. An interesting aspect of this plot is the fact that the PSFs at the ends of the wishbone are closer to each other than they are to the PSFs at the center of the wishbone. This means that that when the PSF is out of focus, flux leaves the core and goes into the halo in a similar, but not identical, way on the two sides of focus.

We have identified 11 general focus zones along the locus of exposures, and grouped the exposures by zone. A few of the exposures lie off the main path. AB17 found that these exposures often correspond to images with jitter or trailing issues. The zone number and the number of exposures in that zone are provided on the figure in green.

5. Constructing a focus-diverse PSF model for F275W

We used the techniques of AB17 to extract a full 7×8 array of fiducial PSFs across the detector for each focus level. Specifically, we copied the exposures for each focus zone into a single directory for that zone. We then identified all objects in each exposure that were (1) unsaturated, (2) had a S/N > 60, and (3) were moderately-well fit by the PSF (this ended up rejecting CRs but not out-of-focus star images). We identified 12,939 stars in the 13 exposures of the first zone, 69,733 in the second-zone exposures, etc. Zone 6 had the most star images at 692,731 in its 94 exposures. Note that while the AB17 study was conducted with the same stars (those in M4), this study involves stars from all over the sky. Many of the exposures come from GO-13297, which is a survey of globular clusters, but there were many other contributing programs as well.

We extracted a 21×21 raster about each star image and recorded those pixels along with the *(x,y)* location in the image as fitted with the PSF. We then took the 13,000 to 700,000 star images in each focus zone and constructed a spatially variable PSF in a manner similar to that in AB17, which itself was based on the approach in Anderson & King (2000, AK00). We solved for the full 7×8 array of fiducial PSFs across the 4096×4096 pixels of the detector. Iteration was required to arrive at the final PSFs since stars are never located at the exact fiducial locations of the PSFs in our models. The PSFs were normalized to have a flux of 1.00 within a radius of 5.0 image pixels. Experience shows that the fraction of light within this aperture does not change significantly with focus.

The PSF for each focus zone was then placed into the "standard" PSF format, described in Anderson (2016). We thus extracted a fully spatially variable PSF for each of the 11 focus zones.

Figure 4 shows contour plots of the spatial array of PSFs for the f=6 focus level for the F275W PSF. The inner 21×21 gridpoints of the ×4-supersampled PSF model are shown, corresponding to the inner 5×5 pixels of star images. The reddest contour at a level of 0.233 is reached at only a few locations on the detector, meaning that all other PSFs never have more than 23.3% percent of their light in their central pixel. Most of the corner PSFs do not even reach a concentration that gets 20% of the light in their central pixels (corresponding to the first cyan contour). These 5×5 pixels are the ones that are most relevant to fit when doing photometry and astrometry with WFC3/UVIS and ACS/WFC. Any variation of the PSF within this aperture will have a large impact on the fitted parameters.

The PSF we have constructed here is a multi-dimensional model, so it is hard to visualize everything at the same time. **Figure 4** showed the PSF at only one focus level (the middle one). **Figure 5** shows the same kind of contour plot as a function of focus parameter, from focus level f=1 on the left to f=11 on the right, for the PSFs at the location identified in the schematic on the left.

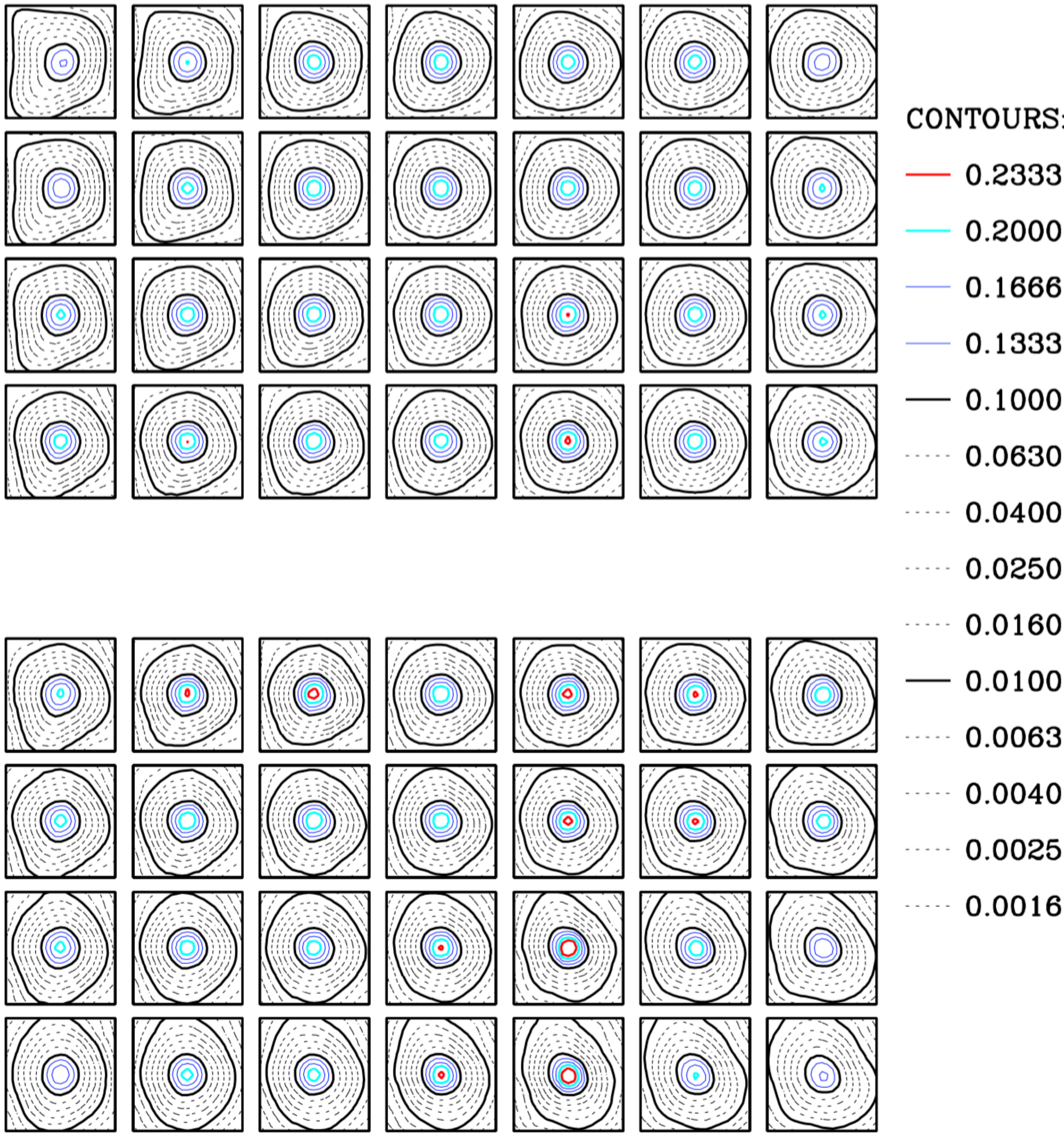

Figure 4: Contour plots of the inner 5×5 pixels for the 7×4 array of PSFs for each chip for the f=6 focus level for F275W. The red contour is the highest, indicating over 23.3% of the star's light in its central pixel. Therefore, the panels that have red at the center represent the places on the detector where the PSF is the sharpest. The region at the bottom edge of the bottom chip has the sharpest PSFs. This corresponds to the "happy bunny" region described in Sabbi & Bellini (2013) and indicated in Figure 1.

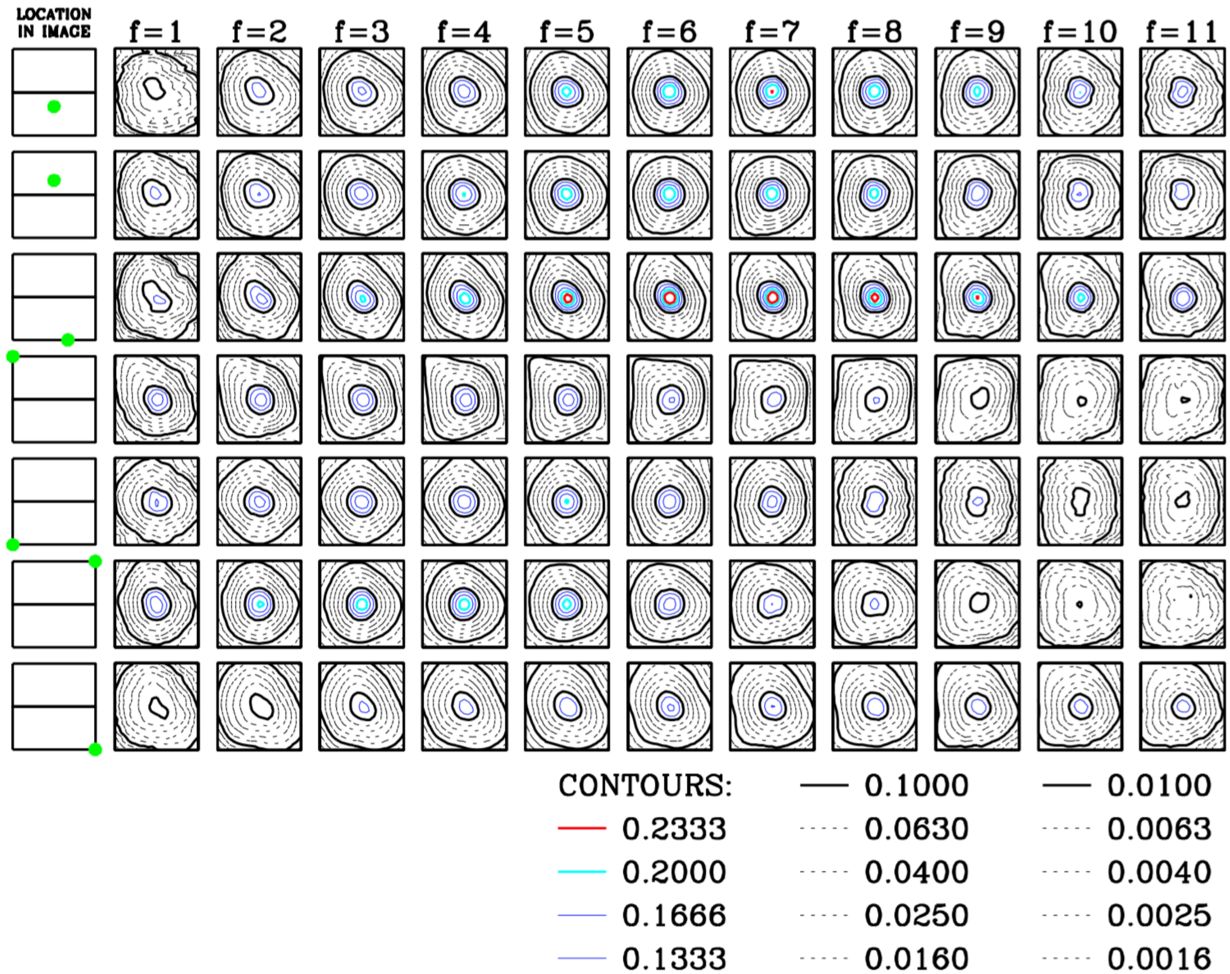

Figure 5: Contour plots showing the inner 5×5 image pixels of the PSF at the detector locations indicated by a green dot in the schematic on the left for PSFs with focus levels from f = 1 through best focus at f = 6 on to f = 11. PSFs with red contours are the sharpest. Those without blue, or even black contours at their centers are extremely distended.

6. STDPBF Format

As mentioned above, the spatially variable PSF for each focus zone was then placed into the "standard" PSF format (STDPSF), described in Anderson (2016), which generated the WFC3/IR PSF in the same format. The STDPSF format is a simple three-dimensional `fits` file with the first two dimensions being 101×101 (corresponding to the Δx and Δy spatial distribution of each fiducial PSF) and a third dimension containing 56 elements, one for each fiducial PSF.

These 11 PSFs were then combined into a single meta-PSF, which, in addition to the 101×101×56 dimensions, has an additional fourth dimension with 11 elements corresponding to the focus level. The STDPBF (**ST**andar**D** **P**sf **B**y **F**ocus) format for WFC3/UVIS thus is a four-dimensional `fits` image with dimensions of 101×101×56×11. These PSFs will be made available shortly, along with software to use them. They have a header similar to that for the STDPSF format, except for the additional keyword for `NAXIS4`.

7. The Other Filters

The previous sections describe the procedure that we used to construct focus-diverse PSFs for the F275W filter. We followed the same procedure for the other four PSFs in this study (F336W, F438W, F606W, and F814W). The four "phylogram" plots are shown on the next page in Figure 6. Note that they are all oriented differently. The orientation is completely arbitrary, since the graph simply represents distances between points.

We constructed full PSFs for each of the indicated zones for each of these filters using the same procedure described in Section 5. We also placed the focus-diverse PSFs into a single STDBPF `fits` file. In **Figures 7** through **10**, we show the behavior of these PSFs as a function of focus for selected locations on the detector.

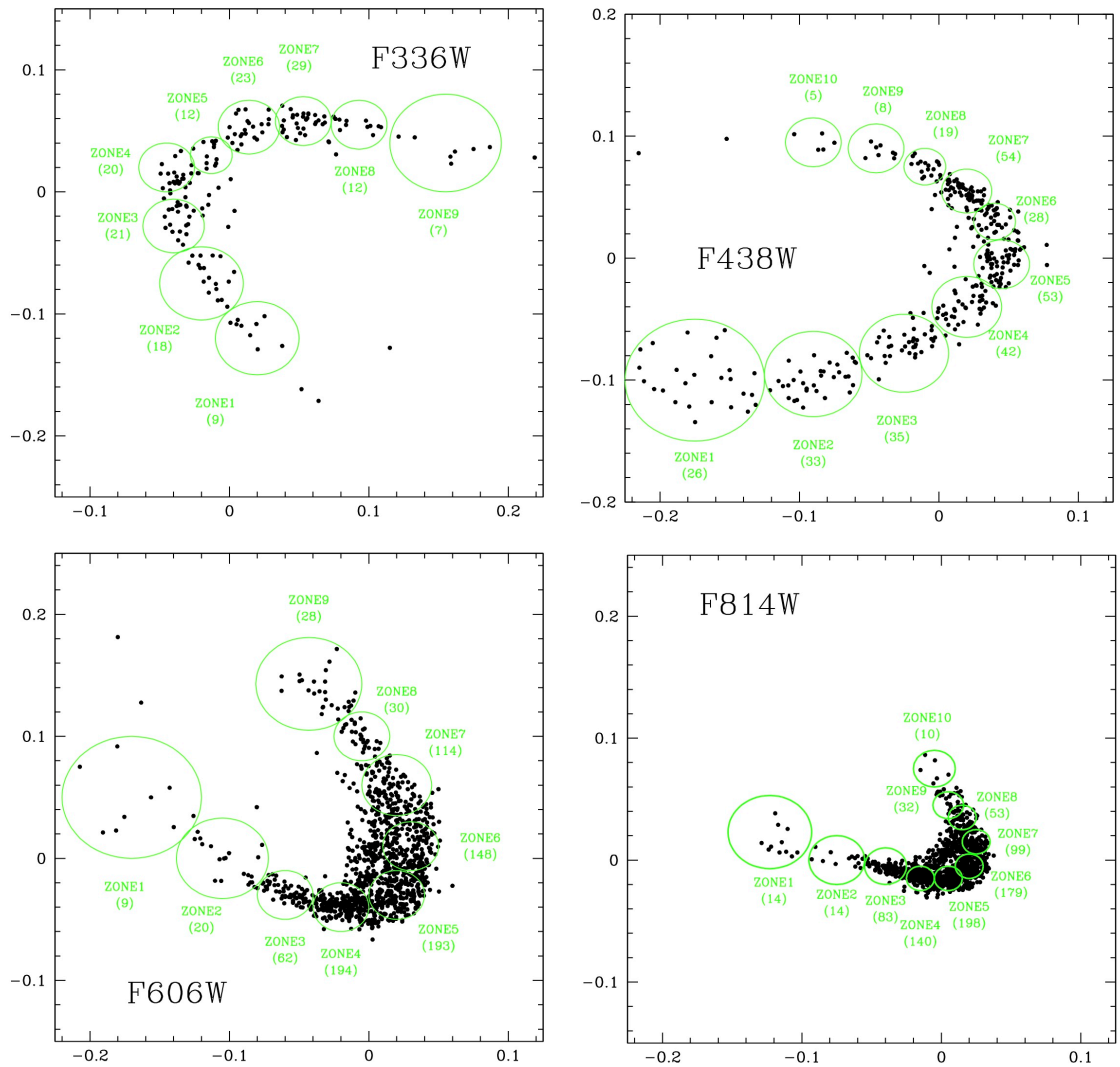

Figure 6: The phylogram plots for the four other filters, along with the zones identified. We identified 9 zones for F336W, 10 zones for F438W, 9 zones for F606W, and 10 zones for F814W. Note that F814W spans a much smaller region of the phylogram plot than the other filters. Clearly the redness of the filter makes it less sensitive than the others to breathing.

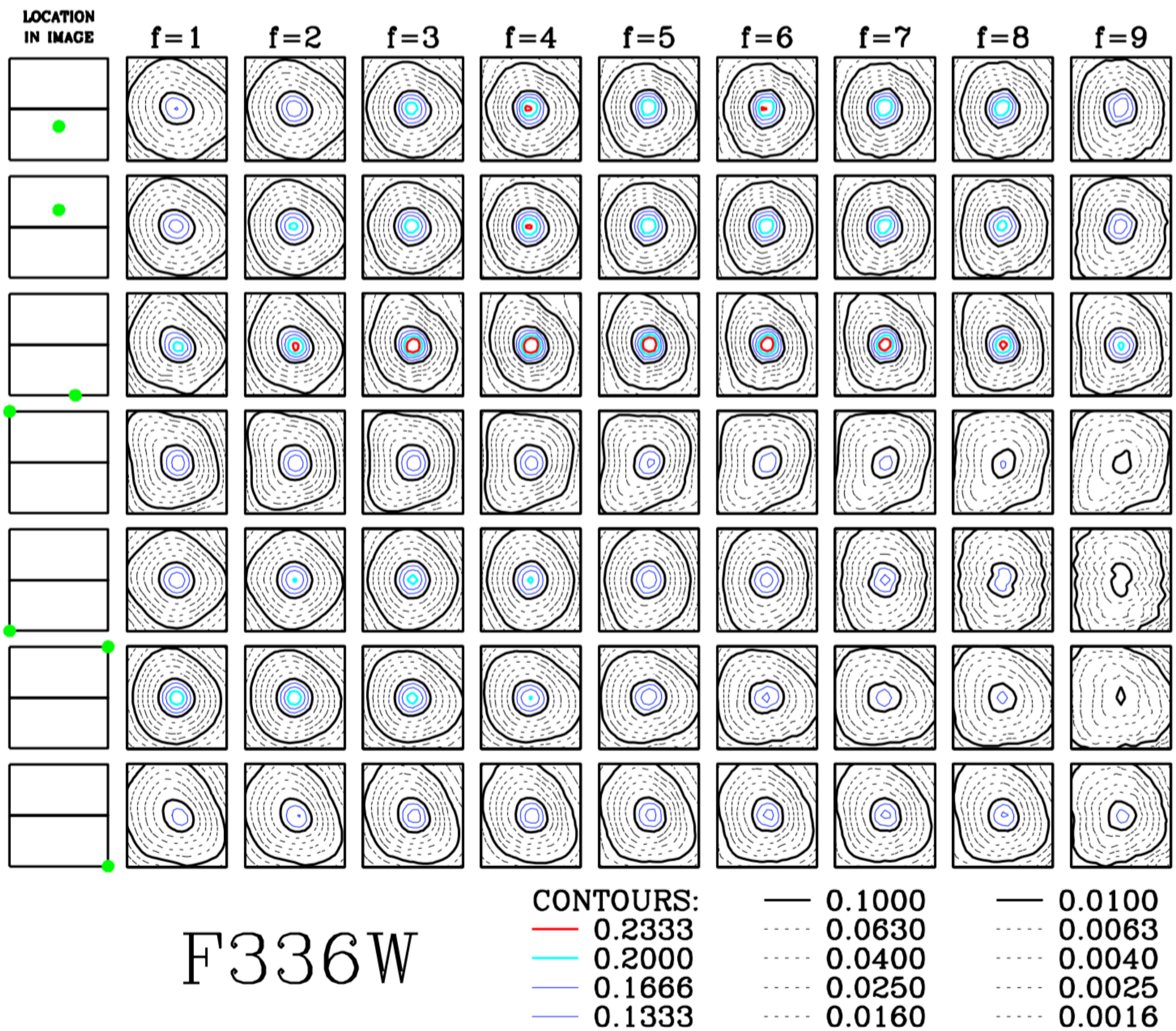

Figure 7: Similar to Figure 5, but for the 9 focus zones of F336W.

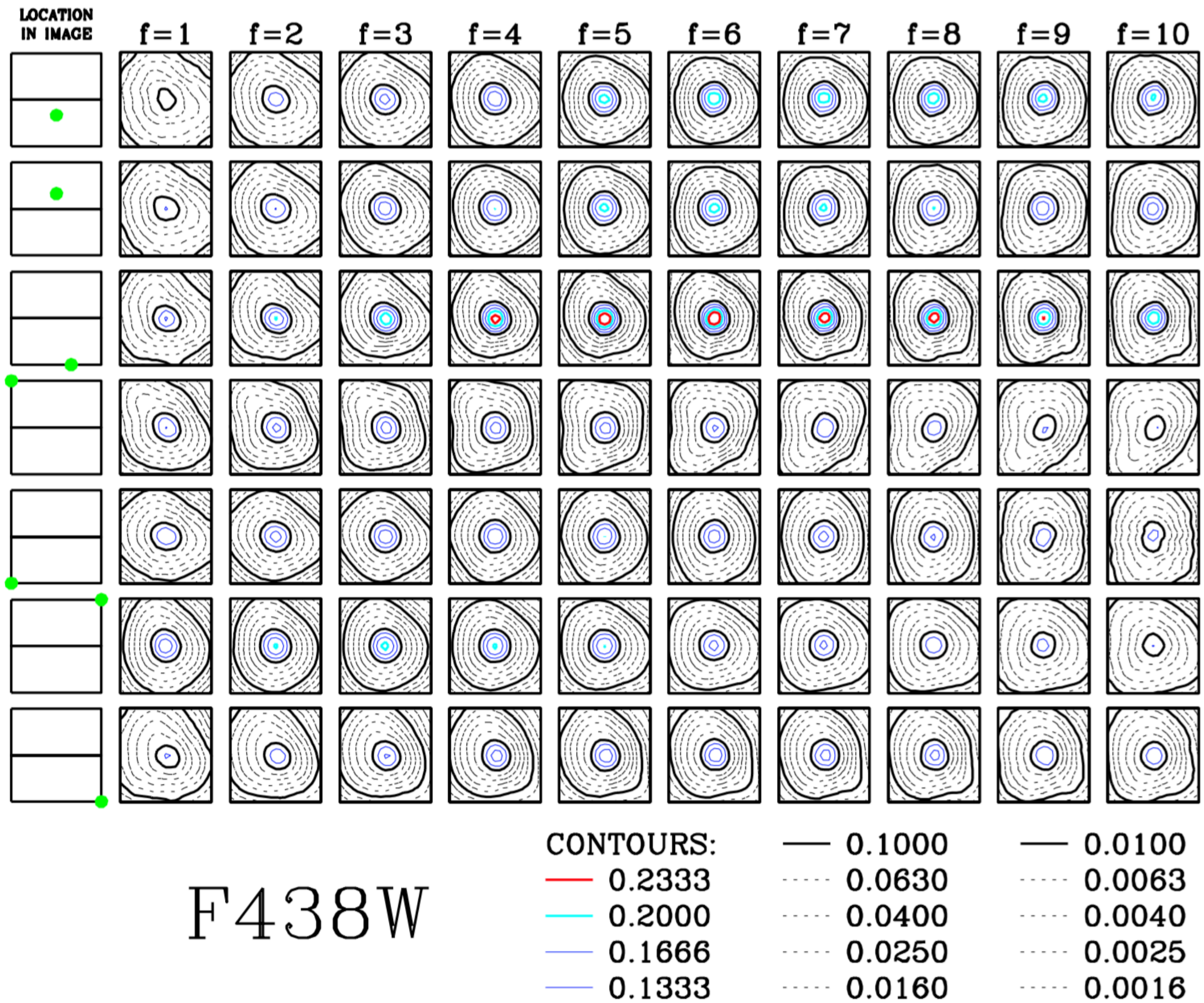

Figure 8: Similar to Figure 5, but for the 10 focus zones of F438W.

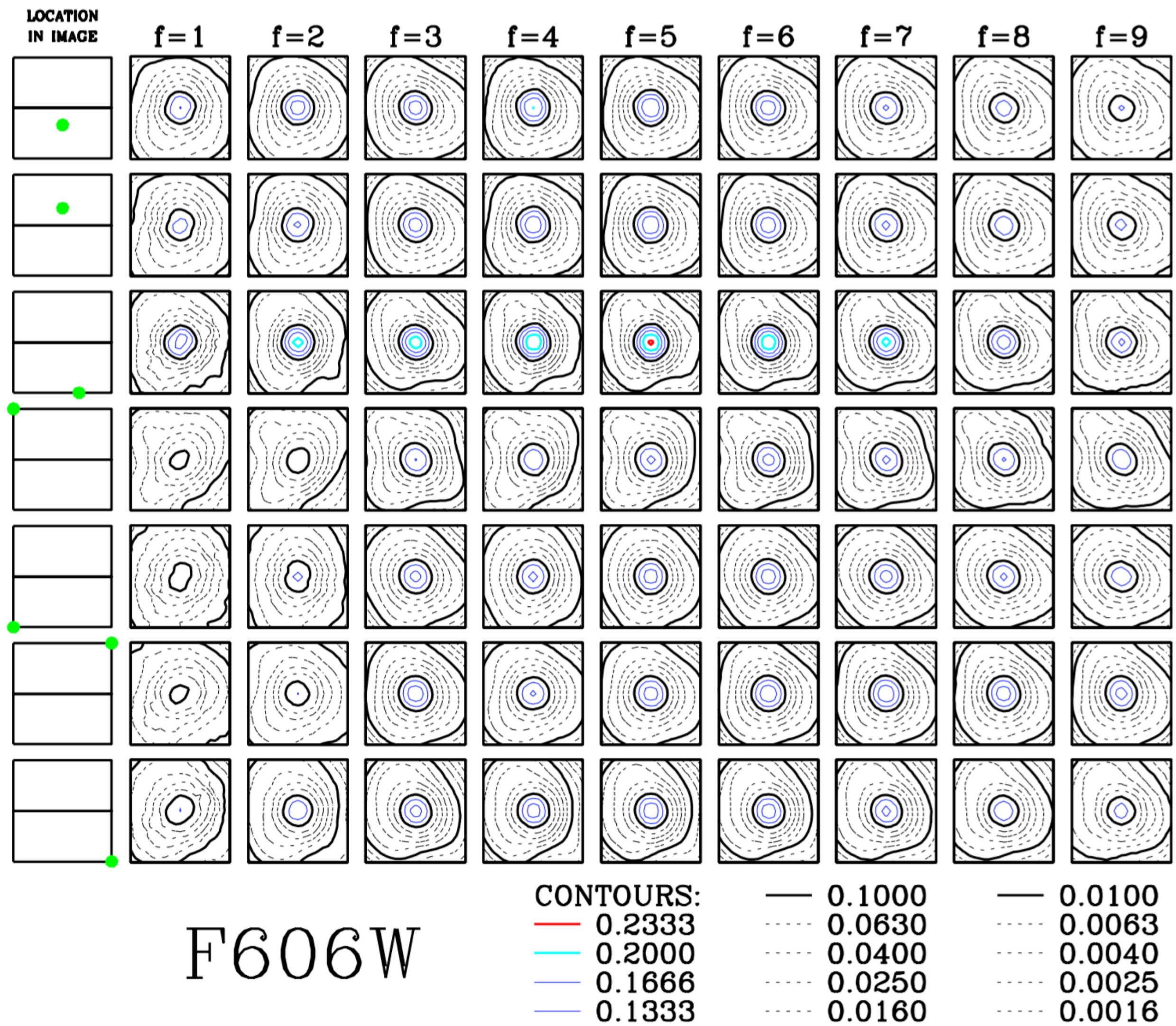

Figure 9: Similar to Figure 5, but for the 9 focus zones of F606W.

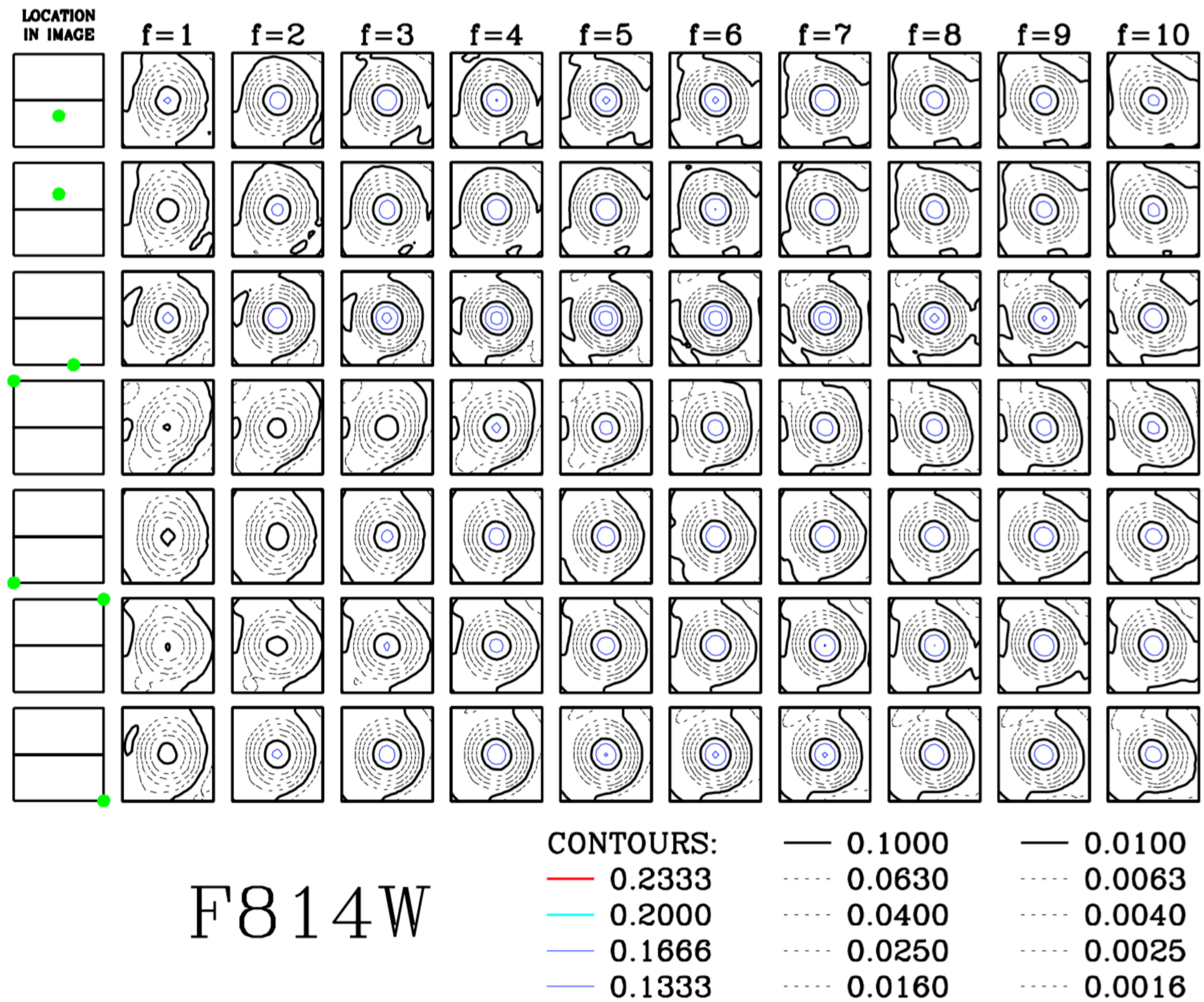

Figure 10: Similar to Figure 5, but for the 10 focus zones of F814W. The contours at the edge of each panel appear to be much flatter than in the previous figures. This is because the F814W PSF is marginally resolved and we are seeing the first airy ring.

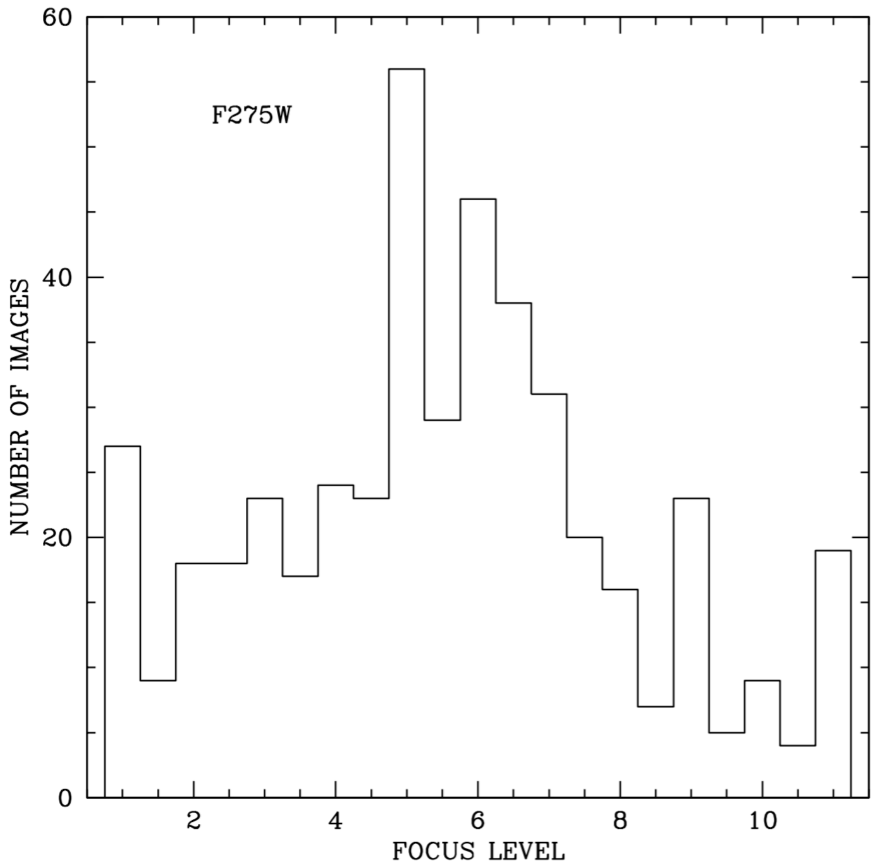

Figure 11: The determined focus level for the F275W images used to construct the PSF.

8. Determining the focus level and PSF for each exposure

Figures 14 and 15 in AB17 show how easy it is to fit for the focus in an image from just a handful of stars. We have been developing a software routine that can be used on WFC3/UVIS images to determine the empirical focus level that best describes the stars in a given exposure, so that an optimal PSF can be constructed for it. Thus far, the routine works only on exposures that have at least 10 stars with S/N>50, but in the next few months, we will be generalizing it to work in a robust way on images that have as few as 5 moderately bright stars. When it is ready, we will release it and the focus-diverse PSFs to the community.

Figure 11 above shows the results from running the preliminary find-focus routine on the images used to extract the F275W PSF. Although PSFs have been derived at only integral locations of the focus level, the routine interpolates the PSFs along the focus curve and assigns a focus for each exposure with a 0.1-level resolution.

9. Next steps

Over the next few months, we will be going through the WFC3/UVIS archive to determine an empirical focus for every exposure made through these filters. We will make this list available to the public and will also use the list, along with phase-retrieval measurements, to better understand HST's focus variations in hopes of making better determinations of when to make focus adjustments. To this end, we have also constructed a focus-diverse set of PSFs for filter F410M, which is the filter that is used for phase-retrieval analysis. These will be presented in an upcoming ISR (Anderson and Dressel 2019).

The PSFs tailored to the focus state of a particular exposure are only part of what users need to analyze the scene in the native, un-resampled `_flc/_flc` frame, where the pixels are true constraints on the astronomical scene. In addition to accurate PSFs, users also need a way to interrelate the pixels of different exposures if they hope to make full use of HST's resolution and sampling.

The BUNDLE structure (Anderson 2014) provides a natural way to do this. A "bundle" is a condensed set of all the information one might need to do a high-precision analysis of an individual object from multiple exposures. The bundle for an object contains an extracted raster centered on that object from the science image in a set of exposures, the error images, and the DQ images. The object may be at different locations on the detector in different images, but the bundle provides the relevant local image data centered on the target. The bundle also contains an empirical mapping from each pixel in each exposure into the reference frame, and vice versa, in order to facilitate a simultaneous analysis of all the constraints on the scene. Finally, the bundle contains an estimate of the local PSF, so that the PSF can be included in a consistent way in a simultaneous analysis of the pixel constraints. Until there were demonstrably accurate PSF models available, the "bundles" had only limited usefulness, but now that we can trust the PSF models better, that makes this kind of analysis more powerful.

In addition to providing software to determine the best PSF for a given exposure, we will also provide a software package (`hst1pass`) that makes use of this PSF to measure sources in HST images. A final software package will use these measured positions to inter-relate the frames of the various exposures so that the pixels of a dithered data set can be analyzed simultaneously using PSF-fitting techniques. Clearly, this involves a great number of inter-dependent routines, but determining accurate PSFs is the first step. The next step will be to provide software that determines focus and uses the best-focus PSF to measure stars.

We anticipate the first routine being released in early 2019, but we wanted to provide the community with a "heads up" that some additional tools are forthcoming. It is likely that the initial routine will be written in `FORTRAN`, but effort is underway to convert various aspects of the package into `python` so that more of the astronomical community can make use of these products in a more flexible way to meet their scientific needs.

Acknowledgements

I am thankful for many useful discussions with the Elena Sabbi, Kailash Sahu, Matthew Bourque, and Linda Dressel. I am also grateful to Linda Dressel for her careful reading of several drafts of this document. In particular, her comments improved the discussion of the how these empirical PSFs might be related to phase-retrieval-derived metrics.

10. References

Anderson, J. *Local Pixel Bundles: Bringing the Pixels to the People*. WFC3/ISR 2014-24

Anderson, J., Bourque, M., Sahu, K., Sabbi, E., & Viana, A. *A Study of the Time Variability of the F606W PSF Images taken with WFC3/UVIS*, WFC3/ISR 2015-08 (A15)

Anderson, J. *Empirical Models for the WFC3/IR PSF*. WFC3/ISR 2016-12

Anderson, J. & Bedin, L. R. *The M4 Core Project with HST — V: Characterizing the WFC3/UVIS PSF by Focus*, 2017 MNRAS 470 948 (AB17)

Anderson, J. & Dressel, L. *The Focus-Diverse F410M PSF for Phase-Retrieval Studies*, WFC3/ISR in progress.

Niemi, S,-M. & Lallo, M., *Phase Retrieval to Monitor HST Focus: II. Results Post-Servicing Mission 4*, HST/TEL ISR 2010-03

Sabbi, E. & Bellini, A. *UVIS PSF Temporal and Spatial Variations*, WFC3/ISR 2011-13